L-valley electron transport in GaAs-AlAs double-barrier resonant tunneling structures studied by ballistic electron emission microscopy

D. Rakoczy,[1] G. Strasser,[1] C. Strahberger,[2] and J. Smoliner[1,*]
[1]*Institut für Festkörperelektronik & Mikrostukturzentrum der TU-Wien, Floragasse 7, A-1040 Wien, Austria*
[2]*Walter Schottky Institut, TU-München, Am Coulombwall, D-85748 Garching, Germany*
(Received 28 March 2002; published 30 July 2002)

Ballistic electron emission microscopy (BEEM) is capable of injecting electrons into the *L* valley of a GaAs-AlAs double-barrier resonant tunneling diode (DBRTD) coherently. Resonant tunneling through the *L*-valley confined states of the DBRTD is then observed as additional current onsets in the BEEM spectrum, followed by a characteristic linear regime. The corresponding ballistic transport mass is derived from the effective-mass tensor by a projection in [100] direction and differs considerably from the GaAs and AlAs longitudinal and transversal effective masses.

DOI: 10.1103/PhysRevB.66.033309 PACS number(s): 73.23.Ad, 07.79.−v, 73.40.Gk, 73.21.−b

Ballistic electron emission microscopy (BEEM) (Ref. 1) is a three-terminal extension of scanning tunneling microscopy (STM), where hot electrons are injected into a semiconductor via a thin metallic base layer. In contrast to STM, BEEM can therefore be used to study subsurface sample properties. BEEM is also capable of detecting higher conduction bands so that, e.g., the energetic position of the *L* and *X* valleys in AlAs can be determined.[2]

For the transport properties of double-barrier resonant tunneling diodes (DBRTD's) the influence of higher valleys cannot be neglected. First tunneling experiments on this topic were carried out by Mendez, Calleja, and Goncalves da Silva[3] who observed resonant tunneling via *X*-point states in AlAs-GaAs-AlAs heterostructures. Later, a DBRTD in the *X*-valley band profile was demonstrated by Sieh and Lee.[4]

In contrast to Γ-X_x transitions (for the definition of the notations see Ref. 5), transitions of electrons between the Γ and *L* valleys are forbidden from the lateral momentum conservation point of view. However, using hydrostatic pressure on GaSb based double-barrier heterostructures,[6] a resonant tunneling of *L*-valley electrons has been demonstrated. On the GaAs-AlGaAs system, *L*-valley resonant tunneling has not been studied experimentally until now, although recent theoretical studies showed that the influence of *L*-valley transport in GaAs-AlGaAs DBRTD's can become observable but strongly depends on the substrate orientation.[7]

In this work, *L*-valley resonant tunneling in GaAs-AlAs heterostructures is investigated by BEEM on [100] oriented samples. Due to the broad momentum distribution of electrons in the metallic base layer, electrons are injected into the *L* valley of GaAs without violating the $k_\parallel$ conservation rules. In this way, we demonstrate the existence of *L*-valley confined states inside the DBRTD and show that the transport mass of *L*-valley electrons in [100] direction is strongly different from the electron effective mass at the bottom of the *L* valley.

For the present experiment, three different molecular-beam epitaxy (MBE) grown GaAs-AlAs DBRTD's were used. All samples were grown on a semi-insulating [100] substrate, on which an n^+-doped GaAs collector was grown, followed by a layer of 1500-Å undoped GaAs. On top of this layer, a DBRTD and a 100-Å-thick protecting GaAs cap layer were grown. The AlAs barriers of all samples were 10 Å thick. The GaAs wells between the barriers were 40, 30, and 20 Å wide, respectively. In addition, a reference sample was grown where the DBRTD structure was replaced by a 100-Å-thick single AlAs barrier.

A schematic view of the experimental setup together with the Γ-conduction-band profile of a DBRTD is shown in Fig. 1(a). Figure 1(b) shows the calculated[8] Γ-, *L*-, and *X*-conduction-band profiles of the sample with a well width of 30 Å. The energetic positions of the higher valleys were taken from Ref. 9. As one can see, a DBRTD exists both in the Γ and the *L* bands, whereas in the *X* band a double quantum well is formed. Note, that a DBRTD is also formed along the GaAs-AlAs-GaAs-AlAs-GaAs Γ-*X*-Γ-*X*-Γ profile. In principle, this should also lead to resonances, since from the $k_\parallel$ conservation point of view, electronic Γ-X_x transitions are allowed. In contrast to that, Γ-*L* transitions are not allowed for transport along the [100] direction, so that no resonances are expected from the DBRTD along the Γ-*L*-Γ-*L*-Γ profile.

To prepare the samples for BEEM experiments, an Au film (70 Å) was evaporated via a shadow mask, giving an active area of 0.2×3 mm^2. Figure 2(a) shows typical experimental data for a temperature of 4.2 K and a tunneling current of 2 nA. In the spectra the lowest current onsets are observed at $V_t = 1.10$, 1.15, and 1.25 V for the sample with well widths of 40, 30, and 20 Å, respectively. Above that onset position, the current increases linearly for all samples. At $V_t = 1.34$, 1.36, and 1.38 V, respectively, a clear second onset is observed in the spectra, which is better resolved in the derivatives of the BEEM spectra shown in Fig. 2(b). In curves 1 and 2 of Fig. 2(b), even a third onset (marked by arrows) is weakly visible. Beyond that, the current increases superlinearly. On the reference sample with the single 100-Å-wide AlAs barrier, no current is detected below $V_t = 1.47$ V, which approximately corresponds to the energetic position of the *X* band at the Au-GaAs interface (marked by the dashed line in Fig. 2). In the derivatives of the BEEM spectra of the DBRTD's, the GaAs *X* band is reflected by a broad shoulder at the same bias position.

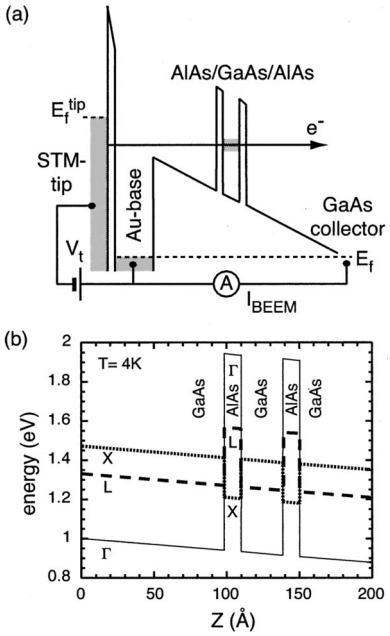

FIG. 1. (a) Schematical view of the experimental setup together with the Γ conduction-band profile of a typical DBRTD sample. The resonant level of the double-barrier structure is indicated by the gray bar. (b) Calculated Γ-, *L*-, and *X*-conduction-band profiles in a sample having a well width of 30 Å.

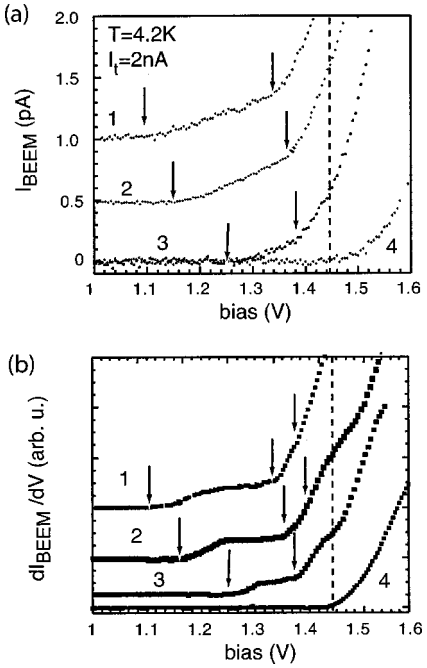

FIG. 2. (a) Typical BEEM spectra obtained experimentally on samples with a GaAs well width of 40, 30, and 20Å, respectively (curves 1–3). Curve 4 was obtained for a sample, where the double-barrier structure was replaced by a single 100-Å-wide AlAs barrier. A current offset was added to the spectra for better viewing. The arrows mark the current onset positions and the dashed line marks the energetic position of the *X* band at the Au-GaAs interface. (b) Derivatives of the BEEM spectra shown in (a).

We first discuss the behavior of the reference sample. Although it is reported in the literature[10] that a BEEM current can be detected as soon as the electron energy is above the AlAs *X* valley [$V_t > 1.22$ V, see Fig. 1(b)], at $T = 4.2$ K we do not detect any current in this regime. This discrepancy can be explained by the fact that most literature data were collected at room temperature. At $T = 300$ K, we also observe a ballistic current above the AlAs *X* valley, whereas at $T = 4.2$ K this current is below the detection limit. Apparently intervalley Γ-*X* transitions at the GaAs-AlAs interface are suppressed at low temperatures.

Although suppressed Γ-*X* transitions at low temperatures were also observed by other groups,[11] an unambiguous explanation for this effect is not given up to now. A possible explanation might be that LO phonons enhance the electron momentum transfer necessary for a Γ-*X* transition. Due to our sample design, the (classical) electron transfer time through our structure is below typical LO-phonon emission times (≈0.1 ps) approximately by a factor of 10, so that Γ-*X* transitions by LO-phonon emission are unlikely in our samples. At low temperatures, the phonon occupation number is small so that phonon absorption cannot enhance the Γ-*X* transition either.

At a first glance, the BEEM spectra of the three GaAs-AlAs DBRTD's look similar to those measured on GaAs-AlGaAs DBRTD's,[12] where a linear increase in the BEEM current is observed between the resonance threshold and the AlGaAs barrier height. This behavior is due to electron refraction at the Au-GaAs interface at the sample surface. An extensive discussion as well as more experimental data concerning this topic can be found in our previous work.[13] However, there are also clear differences; in contrast to the GaAs-AlGaAs DBRTD's, a second current onset is observed, which is followed by a second linear regime. The position of the second current onset is slightly shifted to higher bias with decreasing well width, indicating that this effect is due to a further resonant level inside the well.

To investigate this behavior, we first used a simple one-electron effective-mass model to calculate the resonance positions via a transfer-matrix formalism. As a result, we found that for all samples the measured position of the first onset is in excellent agreement with the calculated resonance position in the Γ-valley profile. The second onset, however, could not be explained with higher levels in the Γ valley, since its energetic position is far below the second calculated Γ-valley resonance for all well widths.

Looking at the band profile in Fig. 1(b), it is straightforward to assume that the second onset is related to the lowest resonant level in the DBRTD formed in the *L* valley of our sample. As Fig. 1(b) shows, we can rule out the possibility that this onset is due to a simple barrier overshoot in higher valleys. First, the AlAs barrier height in the Γ-*X*-Γ-*X*-Γ profile is well below the measured onset positions for all samples. Further, our reference measurements on the single-barrier sample confirm that Γ-*X* transitions can be neglected at 4.2 K. Second, the *X*-band barrier at the Au-GaAs interface is well above the position of the second onset. The *L*-band position at the Au-GaAs interface is in the energy regime of interest, but can also be ruled out since the onsets are shifted to higher bias with decreasing well widths, which

would not be the case for a simple barrier overshoot. Finally, resonant tunneling through the states in the double quantum well in the *X* band can also be excluded, since the embedding barriers are too thick. Therefore, only the resonant level in the *L*-valley DBRTD can be the cause for the second onset.

To verify this further, the transmission coefficients of the DBRTD and the BEEM current were calculated using a semiempirical tight-binding method, which includes the influence of all higher conduction bands and which was already successfully used in our previous experiments.[14] The main results of our calculation can be seen in Fig. 3(a) that shows the transmission coefficients at $k_{\|}=0$ (Γ, X_x solid line) and at a $k_{\|}$ value corresponding to the projected *L* point (dashed line) of the sample band structure (well width 30 Å). The main peak in the solid line at 1.15 eV is due to tunneling processes through the resonant level in the Γ-band profile of the DBRTD. The very narrow resonance structures originate from tunneling through the localized AlAs *X*-valley states. Since the discrete state interacts with a continuum (Fano resonance) a characteristic resonance/antiresonance sequence occurs.[15] The oscillating structure between 1.3 and 1.5 eV is due to interference effects in the region between the Au-GaAs interface and the DBRTD. Tunneling through the second resonant level in the Γ band is not expected before 1.8 eV and therefore is not in the range of interest. In the *L* valley (dashed line), we have resonant levels at energies of 1.32, 1.38, and 1.47 eV. Figure 3(b) shows a comparison of measured and calculated BEEM spectra. Curve 1 shows the measured BEEM spectrum of a 30-Å-well DBRTD and curve 3 the measured BEEM spectrum of the reference sample with the 100-Å-wide AlAs barrier. Curves 2 and 4 are the corresponding calculations. As one can see, the agreement is very good and *X*-valley Fano resonances and interference effects visible in the transmission coefficients do not contribute significantly to the spectrum of the DBRTD.

For the reference sample with the 100-Å-wide AlAs barrier, the calculation [Fig. 3(b), curve 4] yields no significant current below 1.4 V, which is in excellent agreement with the experimental data [Fig. 3(b), curve 3]. This supports our assumption that electronic transitions between the Γ and the *X* valleys are obviously negligible at 4.2 K and that phonons have probably to be involved to observe this effect.

In the last section of this paper we show that a simple effective-mass model and the semiempirical tight-binding model yield equivalent results for the *L*-valley resonance positions, provided the correct ballistic transport masses in [001] direction are used. A similar approach was already utilized by Guthrie *et al.*[16] for Au-Si Schottky diodes.

In resonant tunneling processes only the vertical component of electron momentum enters the transmission coefficient of the DBRTD. If the Fermi energy in the STM tip is swept across a resonant level in the DBRTD, those electrons that are incident vertically ([001] direction) on the DBRTD will determine the resonant current onset, because they have the highest transmission coefficient. In [001] GaAs the growth direction is aligned with the principal axes of the effective-mass tensor for the *X* valleys. Here, the longitudinal, heavy-mass $m^*_{x,1}$ is important for the Γ-*X* transfer and the electron transport in [001] direction. In contrast to that, the

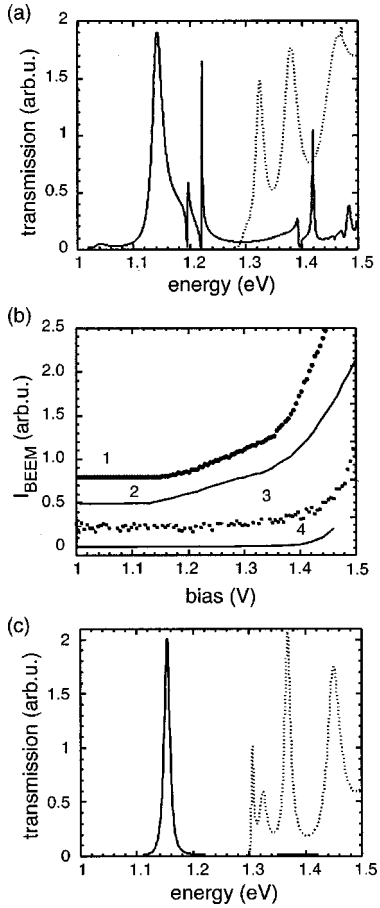

FIG. 3. (a) Results of the tight-binding model for a 30-Å-well DBRTD. The solid line shows the transmission coefficients for $\mathbf{k}_{\|}=0$ (Γ and X_x points). The dotted line is the result for a $\mathbf{k}_{\|}$ at the projected *L* point of the sample band structure. (b) Measured and calculated BEEM spectra. For better comparison the data were scaled and an offset was added. Curve 1 shows a measured BEEM spectrum of a 30-Å-well DBRTD and curve 2 shows the corresponding calculation. Curve 3 shows a measured BEEM spectrum of the reference sample with the 100-Å-wide AlAs barrier and curve 4 shows the corresponding calculation. (c) Transmission coefficients of a 30-Å-well DBRTD calculated with the simple TMM using the correct effective masses in [100] direction. The solid line is the transmission in the Γ-band profile and the dashed line shows the transmission in the *L*-band profile.

principal axes of the *L* valleys, which are in [111] and orthogonal directions, are not parallel to the growth axis and therefore the correct ballistic transport mass must be obtained by a projection from the effective-mass tensor. The energetic positions of the *L*-valley resonance levels are determined by the curvature of the dispersion relation at the *L*-point k_L that can be approximated by

$$E(\mathbf{k})=E_L+\frac{\hbar^2}{2m_0}\sum_{ij}(\mathbf{k}-\mathbf{k}_L)_i\left(\frac{1}{m_L^*}\right)_{ij}(\mathbf{k}-\mathbf{k}_L)_j. \qquad (1)$$

Thus for a structure grown in the [100] direction, the upper left component of $m^{*-1}_{L,ij}$ gives the projected effective

mass for the L valley, $m^{*-1}_{L,[001]}=(1/m^*_L)_{11}$. Due to the symmetry of the band structure, the effective-mass tensor at the L point has the general form

$$\frac{1}{m^*_L}=\begin{bmatrix} a & b & b \\ b & a & b \\ b & b & a \end{bmatrix}. \tag{2}$$

The parameters $(a;b)$ are obtained by the tight-binding model. If we insert them into Eq. (2), we get values of $m^*_{L,[001]}=0.172$ in GaAs and $m^*_{L,[001]}=0.234$ in AlAs, which differ considerably from the longitudinal (m_l) and transversal (m_t) masses in both materials (see Table I).

To verify that a simple effective-mass model and the semiempirical tight-binding model can yield equivalent results, provided the correct ballistic transport masses in [001] direction are used, the above m^* values were used as input for our simple TMM program and the transmission of the Γ- and L-valley band profiles were calculated. As one can see, there is a reasonable qualitative agreement between the semiempirical tight-binding model [Fig. 3(a)] and the simple TMM with the correctly projected masses [Fig. 3(c)]. However, even with the correctly projected masses there are also some clear differences in the results. First, the peaks due to Fano resonances do not exist in the simple model. Second, the very sharp small peak at 1.3 V is only observed in the TMM calculation. This is an artifact due to resonant tunneling through a state in the triangular well formed between the Au-GaAs interface and the first AlAs barrier. In the semiempirical tight-binding model, this is just observed as a shoulder on the left side of the first L-valley resonance. Finally, the structures in the Γ-valley transmission above 1.35 V are not reproduced by the simple model. This clearly shows that if the correct projected mass is known, a simple TMM can be useful for a first estimate of resonance positions also in higher valleys. On the other hand, finding the origin of unknown structures in the BEEM spectra will require more sophisticated simulations.

TABLE I. Effective masses at the Γ, X, and L valley of GaAs and AlAs, and the parameters $(a;b)$ as obtained by the semiempirical tight-binding model.

GaAs			
Symmetry point	Γ	X_x	L
m_l	0.067	1.14	1.66
m_t		0.276	0.119
$m_{[100]}$		0.276	0.172
$(a;\ b)$			(5.8; −2.6)
AlAs			
Symmetry point	Γ	X_x	L
m_l	0.162	1.38	1.76
m_t		0.263	0.164
$m_{[100]}$		0.263	0.235
$(a;\ b)$			(4.26; −1.85)

In summary, we have investigated resonant tunneling through quantized states in the L valley of a double-barrier resonant tunneling diode. Due to the broad momentum distribution in the Au-emitter electrode, BEEM is capable of injecting electrons into the L valley of the structure coherently. For this reason, resonant levels in the L valley of the DBRTD manifest themselves in the BEEM spectrum as additional current onsets followed by a characteristic linear regime. Using a semiempirical tight-binding method, the ballistic transport mass was derived from the effective-mass tensor by a projection in [001] direction. It turned out that it differs considerably from the GaAs and AlAs longitudinal and transversal effective masses.

This work was sponsored by FWF Project No. P14604-TPH and Gesellschaft für Mikroelektronik (GMe). The authors are grateful to E. Gornik and P. Vogl for continuous support.

*Email address: juergen.smoliner@tuwien.ac.at

[1] W. J. Kaiser and L. D. Bell, Phys. Rev. Lett. **60**, 1406 (1988).
[2] W. J. Kaiser, H. Hecht, L. D. Bell, F. J. Grunthaner, J. K. Liu, and L. C. Davies, Phys. Rev. B **48**, 18 324 (1993).
[3] E. E. Mendez, E. Calleja, and C. E. T. Goncalves da Silva, Appl. Phys. Lett. **50**, 1263 (1987).
[4] Tung-Ho Sieh and Si-Chen Lee, Appl. Phys. Lett. **63**, 1219 (1993).
[5] O. Madelung, M. Schultz, and H. Weiss, *Physics of Group IV Elements and III–V Compounds*, Landolt Börnstein, New Series, Group III, Vol. 17a (Springer-Verlag, New York, 1982).
[6] J. L. Jimenez, E. E. Mendez, X. Li, and W. I. Wang, Phys. Rev. B **51**, 7938 (1995).
[7] Jiann-Shing Shyu and Jih-Chen Chiang, Phys. Rev. B **60**, 1799 (1999).
[8] G. Snider, *1D Poisson* (University of Notre Dame Press, Notre Dame, IN, 1995); URL: www.nd.edu/~gsnider/
[9] J. M. Mancu, R. Scholz, F. Beltram, and F. Bassani, Phys. Rev. B **57**, 6493 (1998).
[10] Mao-Long Ke and D. I. Westwood, Appl. Surf. Sci. **123/124**, 255 (1998).
[11] J. J. O'Shea, E. G. Brazel, M. E. Rubin, S. Bhargava, M. A. Chin, and V. Narayanamurti, Phys. Rev. B **56**, 2026 (1997).
[12] T. Sajoto, J. I. O'Shea, S. Bhargava, D. Leonard, M. A. Chin, and V. Narayanamurti, Phys. Rev. Lett. **74**, 3427 (1995).
[13] J. Smoliner, R. Heer, C. Eder, and G. Strasser, Phys. Rev. B **58**, 7516 (1998).
[14] C. Strahberger, J. Smoliner, R. Heer, and G. Strasser, Phys. Rev. B **63**, 205306 (2001).
[15] T. Ando, S. Wakahara, and H. Akera, Phys. Rev. B **40**, 11 609 (1989).
[16] D. K. Guthrie, L. E. Harrel, G. N. Henderson, P. N. Fist, T. K. Gaylord, E. N. Glytsis, and R. E. Leibenguth, Phys. Rev. B **54**, 16 972 (1996).